Nuclear Magnetic Interactions in Hydrogen Fluoride*

MILTON R. BAKER, H. MARK NELSON,† JOHN A. LEAVITT,‡ AND NORMAN F. RAMSEY
Harvard University, Cambridge, Massachusetts

(Received September 16, 1960)

The radio-frequency spectra corresponding to the reorientation of the proton and fluorine nuclear magnetic moments in hydrogen fluoride (HF) have been observed in fields of 900, 1800, and 3600 gauss by means of the molecular beam resonance method. Details are presented on the design and construction of the new molecular beam apparatus and electron-bombardment detector used in the experiment. The theory of the HF strong-field energy levels is outlined, and the expected proton and fluorine transitions derived for $J=0$, 1, and 2 are tabulated. From the observed resonance shapes, one can deduce the magnitudes of the spin-rotational interactions of the proton and fluorine nuclei, and their spin-spin interaction. These are: $|c_p| = 71 \pm 3$ kc/sec, $|c_F| = 305 \pm 2$ kc/sec, $d_1 = 57 \pm 2$ kc/sec. The correctness of these parameters was checked by the good agreement between the experimental curves and resonance shapes predicted by Univac programs using these values. The observed fluorine spin-rotational interaction constant is the largest yet observed and corresponds to a rotational magnetic field at the nucleus of 76 gauss per unit rotational quantum number. The implications of the large spin-rotational interaction for relaxation processes in nuclear magnetic resonance experiments are discussed.

I. INTRODUCTION

THE method of molecular beam magnetic resonance furnishes a highly effective means for studying the Zeeman hyperfine structure of molecules. Experimentally, detection of the molecular beam after it has passed through the magnetic or electric deflection and transition fields has in the past limited the scope of the method. A detector utilizing ionization of the molecular beam by electron bombardment possesses the advantages of wide applicability and fast response time. Such a detector was first used for condensable beams by Wessel and Lew,[1] and was adapted to noncondensable beams by Quinn *et al.*[2] who used it in their studies of HD.[3]

A versatile new molecular beam magnetic resonance apparatus incorporating an improved electron-bombardment detector has been recently constructed, in order to widen the range of molecules which can be studied. The apparatus is described in detail in Sec. II. The first investigations carried out on it have been concerned with the nuclear magnetic spectra of hydrogen fluoride (HF), in fields of from 900 to 3600 gauss. This $^1\Sigma$ molecule has not been previously examined by the molecular beam method or by any other method that can provide similar information. The nuclear magnetic moments of the proton and fluorine nuclei in the molecule are large, which permits a comparatively easy deflection in the A and B fields. The nuclei are both spin $\frac{1}{2}$, simplifying the analysis of the spectrum by minimizing the possible nuclear orientations in the external field. A small moment of inertia of the molecule allows the lower rotational states to be thermally populated. These characteristics seemed particularly suitable for initial experiments with a new apparatus.

From the observed transition frequencies and spectral shapes can be deduced the values of several of the constants which appear in the molecular hyperfine Hamiltonian. In particular, the magnitudes of the spin-rotation constants, which depend on the molecular free rotation and which are averaged to zero in non-molecular-beam resonance experiments, were obtained. The Hamiltonian used is similar to that which has been given for the hydrogen molecule, and no unexpected interaction was required to interpret the data. The strong-field energy levels and transition frequencies obtained from them for molecular rotational states $J=0$, 1, 2 are presented in Sec. III. In the case of HF, individual transitions have not yet been resolved. Since the number of possible transitions becomes large, interpretation was facilitated through the use of an electronic computer to predict resonance shapes for different values of the input parameters. Several Univac programs have been so devised, and have proven highly useful in determining the best choice of molecular-interaction constants.

There has been a large amount of recent theoretical work on the electronic structure of diatomic molecules, and, particularly, of HF.[4] High-speed machine computation has enabled the wave functions to be obtained with considerable accuracy. From this, the value of experimentally measurable quantities, such as the electric dipole moments and electric field gradients, can be calculated directly. Other calculations are in progress using the wave functions as the bases for variational calculations to include the effects of perturbation-introduced excited states, such as are involved in the nuclear diamagnetic shielding, spin-rotational interactions, and rotational magnetic moments. The experimental values of these quantities furnish criteria for evaluating the

* This work was supported in part by the National Science Foundation and the Joint Program of the Office of Naval Research, and the U. S. Atomic Energy Commission.

† Present address: Brigham Young University, Provo, Utah.

‡ Present address: University of Arizona, Tucson, Arizona.

[1] G. Wessel and H. Lew, Phys. Rev. **90**, 1 (1953).

[2] W. E. Quinn, A. Pery, J. M. Baker, H. R. Lewis, N. F. Ramsey, and J. T. LaTourrette, Rev. Sci. Instr. **29**, 935 (1958).

[3] W. E. Quinn, J. M. Baker, J. T. LaTourrette, and N. F. Ramsey, Phys. Rev. **112**, 1929 (1958).

[4] Revs. Modern Phys. **32**, No. 2 (1960).

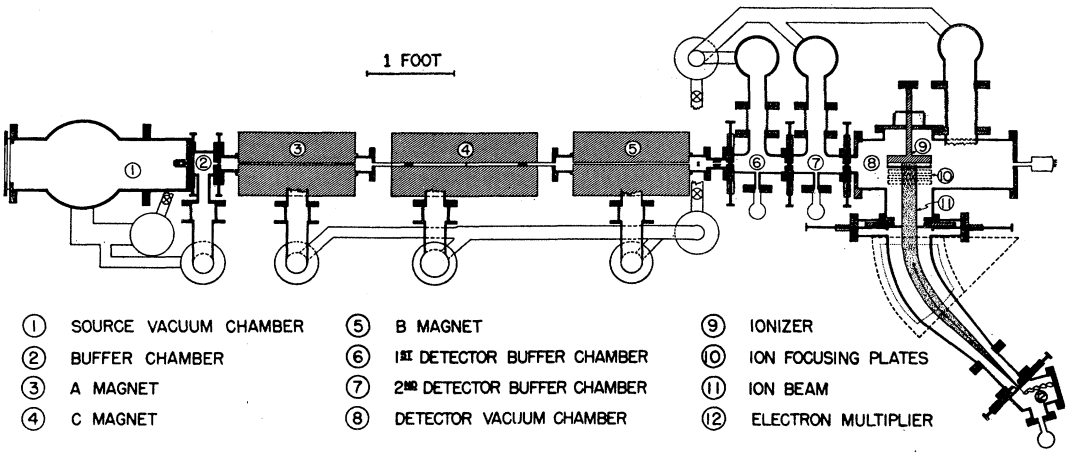

FIG. 1. Top view of the molecular beam apparatus.

techniques developed for many-electron molecular problems, and determining their limitations.

II. APPARATUS

To produce the conditions under which transitions may be induced and detected in a beam of molecules requires an array of vacuum and electrical equipment. The point of view adopted in this description will be to emphasize the features peculiar to this apparatus, since many standard design considerations are now quite completely discussed in the literature.[5] Distinguishing characteristics of this apparatus are:

(a) the use of detachable vacuum sections to facilitate changing experimental conditions, such as the length of the C field;

(b) magnets either wholly or mostly external to the vacuum envelope;

(c) the use of a 25-foot long aluminum H beam, on which the equipment is mounted, to furnish rigidity against deflections in the manner of an optical bench.

(d) utilization of electronically-regulated high-voltage supplies with high-impedance magnet windings for the deflection and C field;

(e) an electron-bombardment ionization detector, which bombards the molecular beam over a 10-cm length;

(f) a mass spectrometer of very wide aperture to analyze the ion beam;

(g) a stainless steel, copper-gasketed, detector vacuum system, which can be baked out at high temperature, and is pumped by mercury diffusion pumps.

A scaled top view of the apparatus is shown in Fig. 1. The gas to be studied is introduced through a gas-handling system into the source, which is suspended into the vacuum from an Invar cold trap, and whose temperature can be adjusted by filling the trap with liquids. The beam is produced by the effusion of gas from the source, which is kept at about 5 mm Hg pressure. It passes through a thin vertical slit into the lower vacuum of the source pumping chamber. In accordance with the classic Rabi method, the beam of molecules then passes through successive regions of magnetic fields and is incident on a detector slit. By means of a collimating slit, located at the center of the C magnet and whose width is comparable to that of the source slit, the beam is confined to a width of 0.005 cm and a height of about 0.8 cm.

The inhomogeneous A field deflects the path of a molecule by acting on its effective magnetic moment with a field gradient of from 10 to 30 kgauss/cm. The inhomogeneous B-field gradient is oppositely directed to that of the A field and so refocuses the beam on a slit located in front of the beam detector. If, in the C-field region, transitions are induced from one molecular energy level to another with differing effective magnetic moment, the molecules will no longer be refocused. Thus, the beam intensity registered will decrease whenever there is such a transition induced within the C-field region. This occurs when the small oscillatory magnetic field in the rf coils, which is applied parallel to the beam and perpendicular to the C field, has a frequency related by the Bohr condition to the energy differences between the initial and final states.

The vacuum in the large chamber surrounding the source is maintained at about 10^{-5} mm Hg by a Consolidated Vacuum Corporation (CVC) pump, type MCF-1400, surmounted by an integral freon-refrigerated baffle.[6] Half-inch adjustable channel slits are used between the source, buffer, and A-magnet sections so that the main chamber pressure may be kept independent of the source efflux by the use of differential

[5] N. F. Ramsey, *Molecular Beams*, (Oxford University Press, New York, 1956).

[6] Details of the construction methods, dimensions, and circuitry used can be found in M. R. Baker, thesis, Harvard University, 1960 (unpublished); H. M. Nelson, thesis, Harvard University, 1959 (unpublished); J. Leavitt, thesis, Harvard University, 1960 (unpublished).

pumping. The buffer chamber is pumped by a CVC, MCF-300 fractionating oil pump and its usual operating pressure is 2×10^{-6} mm Hg. At the entrance of the *A*-magnet vacuum chamber is a sliding valve using an O-ring seal actuated by an eccentric shaft, which permits the source and buffer chambers to be separated from the main chamber if desired. The common source-buffer foreline pressure is maintained by a booster diffusion pump (CVC, MB-100) and a Welch 1397*C* mechanical pump. Use of the booster pump caused a noticeable improvement in the performance of the MCF-1400.

The main chamber is composed of the vacuum envelope made by connecting together the *A*, *C*, and *B* magnet vacuum chambers. The *C* magnet is entirely external to its vacuum envelope. The molecular beam runs down the center of the $\frac{1}{2}$-in. gap between the *C*-magnet pole pieces, and is enclosed in a rectangular brass tube $\frac{1}{2}$ in.$\times$2 in. in cross section. To provide sufficient pumping speed from this small volume to the diffusion pump, a pumping manifold of $1\frac{3}{4}$-in.$\times$4-in. rectangular brass tubing is silver-soldered onto the top of the beam tube. A 3-in. side pipe leads through a liquid N_2 trap to an MCF-300 diffusion pump. O-ringed ports for the collimator and rf coils are provided on the top, while end flanges permit bolting together with the *A* and *B* vacuum sections.

The *A* and *B* vacuum sections are identical, and closed by the sealing action from the side of flanges integral to the *A* and *B* magnet pole pieces onto O rings in rectangular grooves. These grooves are machined around the sides of the two rectangular brass tubes through which the pole pieces fit. The high magnetic field gradients required in the *A* and *B* magnets necessitate small gaps between the pole tips, which are of the bead and groove, two-wire field type.[5] The small cross section and odd shape of the gap precluded the use of a thin tube, pumped from its ends. The vacuum-tight box formed by the *A* or *B* pole piece inserted into the rectangular tubing is surmounted by a pumping manifold similar to the one used in the *C* envelope. The manifolds have integrally mounted liquid N_2 traps. Forelines of the *A*, *B*, and *C* envelope diffusion pumps are pumped by an MB-100 booster and a second Welch 1397*C* mechanical pump. The vacuum maintained in the main chamber under normal operating conditions is about 5×10^{-7} mm Hg.

The apparatus is mounted on a large aluminum *H* beam which serves to prevent relative motion of the individual components of the vacuum system. It is composed of 3 plates of 6061-ST aluminum, 1 in. thick and 25 ft long, assembled by heliarc welding. The *H* beam is supported on two concrete pillars 16 ft apart by rubber shock mountings, to prevent vibration from neighboring reciprocating machinery from disturbing it. This method of mounting causes any distorting force to be transmitted to the *H* beam as a whole, and pushing sideways on the mount causes no observable change in the intensity of a collimated molecule beam. Leveling and positioning the source, collimator, and magnets with respect to the mounting beam are provided by screws and pads set in the aluminum.

The *C*-field magnet is 9 in. square in cross section, 20 in. long, and made of heat-treated, forged, Armco magnet iron. The yoke pieces are $2\frac{1}{2}$ in. thick, and the various rectangular slabs which form the magnet are assembled by means of iron studs. The *C*-field pole tips are $2\frac{1}{2}$ in. high, with an air gap of $\frac{1}{2}$ in., which is kept highly uniform by careful surface grinding and assembly of the slabs. The *A* and *B* field magnets are similar in construction and material, except that they are 16 in. long and have bead-and-groove pole tips with radii of $\frac{3}{16}$ in. and $\frac{7}{32}$ in., respectively. The bead and part of its pole tip are made of vanadium permendur (Western Electric), fastened by DeKhotinsky cement to the yoke. Short, tapered end sections on the *A* and *B* magnet pole tips prevent nonadiabatic (Majorana) reorientations of the molecular magnetic moments.

The *C* field is excited by two coils, each of which consists of 5000 turns of No. 26 Alkanex wire. The coils were wound on water-cooled copper coil forms, and then vacuum potted in Al_2O_3-filled epoxy resin to improve heat conduction from the windings. The *C* field produced by putting the coils in series is about 10 000 gauss/ampere up to 1 ampere. The set of four coils which excite the *A* and *B* magnets are similar in construction to the *C* magnet coils but are wound with 3000 turns of No. 22 Formex wire each.

Power for the windings of the magnet coils is supplied by two electronically voltage-regulated power supplies, which furnish up to 1.5 amperes of current at 1200 volts. These utilize 3-phase, full-wave rectification, and a difference-amplifier regulator with a dc stabilization ratio of 15 000. To achieve magnetic field stabilities of 2–5 parts in 10^6, current regulation is performed in two steps. The supply voltage is first stabilized to about 1 part in 10^4 by the voltage regulator using stacked 85*A*2 reference tubes. After passing through dropping and control resistors, which are mounted in a large, water-cooled decade box, the current passes through the magnet windings and one of several different manganin wire resistors. The voltage drop across the manganin is compared with that of stacked standard cells by means of a Brown amplifier. Shunt vacuum tubes controlled by the Brown amplifier keep the current constant by acting as variable resistors in series with the magnet windings. The low current, high-voltage magnet supplies, instead of the high-current submarine batteries customarily used, have facilitated operations such as demagnetization and changing connections, while permitting long runs to settle down the magnets.

Radio-frequency current for the two oscillatory-field coils is supplied by a radio-transmitter of standard design (Millen No. 90881) operating in the range 1.6 to 30 Mc/sec. The source of excitation is either a surplus Navy ATD aircraft transmitter, or a variable-frequency

oscillator and exciter-unit (Millen No. 90711 and 90801). The rf coils are inserted 2 in. in from each end of the C field. They consist of 8 turns each of $\frac{1}{16}$-in. o.d. copper tubing wound on a rectangular polystyrene form and supported from their O-ring sealing flanges by brass fixtures. The coil dimensions are: $\frac{7}{8}$ in.$\times\frac{1}{4}$ in. in cross section; $\frac{3}{4}$ in. in length. In place, they fit snugly between the walls of the $\frac{1}{2}$-in. wide C-magnet beam envelope tube, whose grounded walls act as rf shields. Water cooling is introduced into the thin copper tubing outside the vacuum through polyvinyl tubing. During a run, the frequency of the rf current is swept by means of a variable-speed motor, while being monitored with a frequency counter (Northeastern Engineering, model 14–20 AT).

The electron-bombardment detector incorporates several features which were found to be necessary for use with noncondensable beams during previous experiments. These are: (1) buffer chambers and channel slits before the detector to prevent nonbeam source gas from diffusing to the detector; (2) a mass spectrometer to discriminate against masses differing from those of the beam molecules; and (3) modulation of the beam and synchronous (lock-in) detection. Concentration of the electron beam and the reduction of background pressure in the detector to a minimum are also paramount factors.

High background arising from the use of oil diffusion pumps had been a source of difficulty in earlier electron-bombarder detectors, because of the tendency of pump oil to break up into mass fractions of almost every integral mass number. This dictated the use of Hg diffusion pumps, with continuous liquid nitrogen and freon baffling. The envelope of the detector vacuum system is entirely constructed of heliarc-welded type 304 stainless steel. Detachable seals on flanges are made by OFHC hydrogen-fired copper shear gaskets of the Lange-Alpert type. Two buffer chambers and three sets of channel slits precede the bombardment region. The

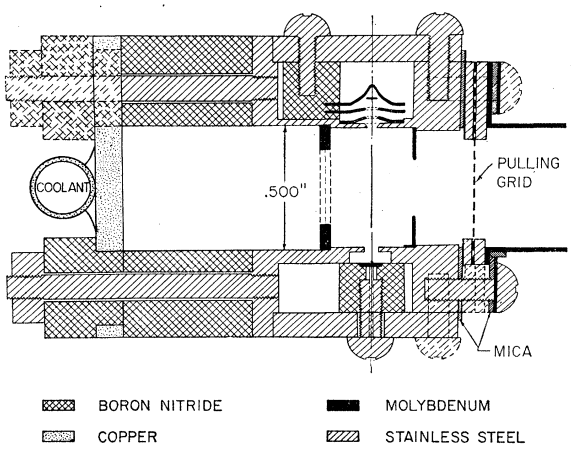

FIG. 2. Cross section of the bombardment region of the electron-ionization detector.

TABLE I. Typical operating conditions of the electron bombardment detector.

Filament backing grid	0 v
Space-charge control grid	25 v
Box and second accelerating grid	250 v
Collector voltage	280 v
Total emission	50 ma
Collector current	10 ma
Ion pulling voltage (relative to the box)	−30 v
Filament current (0.040-in.×0.002-in. Th-W ribbon)	7 amp

common forelines of the three detector pumps (2 MHG-180, 1 MHG-300, CVC) lead to an MHG-50 Hg booster pump, which is pumped in turn by the Welch mechanical main-chamber pump. In a previous electron bombarder,[2] back diffusion precluded the use of a common foreline for the buffer and detector chambers. The use of a booster pump to reduce foreline pressure completely eliminated the difficulty in the present detector. After bake-out, operating pressures of from 1 to 4×10^{-9} mm Hg have been obtained in the detector chamber.

The bombardment region is shown in Fig. 2 in cross section. It consists of a stainless steel box, 6 in. long and 1 in. square, which is supported from a bellows flange by insulators of boron nitride.[7] In the upper face is a removable mounting plate for the electron gun, which is of the two-dimensional Pierce type. The electrons, after emission from a 4-in. Th-W filament are focused and accelerated by shaped Mo grids into a field-free region. After passing vertically downward through the molecular beam, which enters through the front of the box, the electrons are collected on a recessed Mo anode.

On the side of the box is a pulling grid, insulated from the box and negative with respect to it. The ions produced are thus extracted and pass through 3 pairs of parallel-plate condensers which act as cylindrical, saddle-type, electrostatic lenses to deflect and focus the 4-in. wide ion sheath in the vertical direction. Table I shows typical bombarder operating conditions. Voltages for acceleration and focusing are provided by a circuit similar to that described in reference 2, while the electron gun filament and beam currents are supplied by regulated power supplies fed through isolation transformers. The bombardment box can be independently rotated about the three perpendicular axes through its center and translated sidewards by motions which are introduced into the vacuum through sylphon bellows and micrometer heads. Electrical connections to the interior are made by ceramic-metal seals (Advanced Vacuum Product Company) which have proven superior in ruggedness to Kovar-glass seals.

Mass analysis of the ion-beam is performed by a sectorial-field mass spectrometer designed to focus a wide horizontal beam of ions moving parallel to each

[7] This substance has proven highly useful in the construction of the bombarder, because of its properties of easy machinability, excellent electrical resistivity at high temperatures, high thermal conductivity, low vapor pressure, and low coefficient of friction.

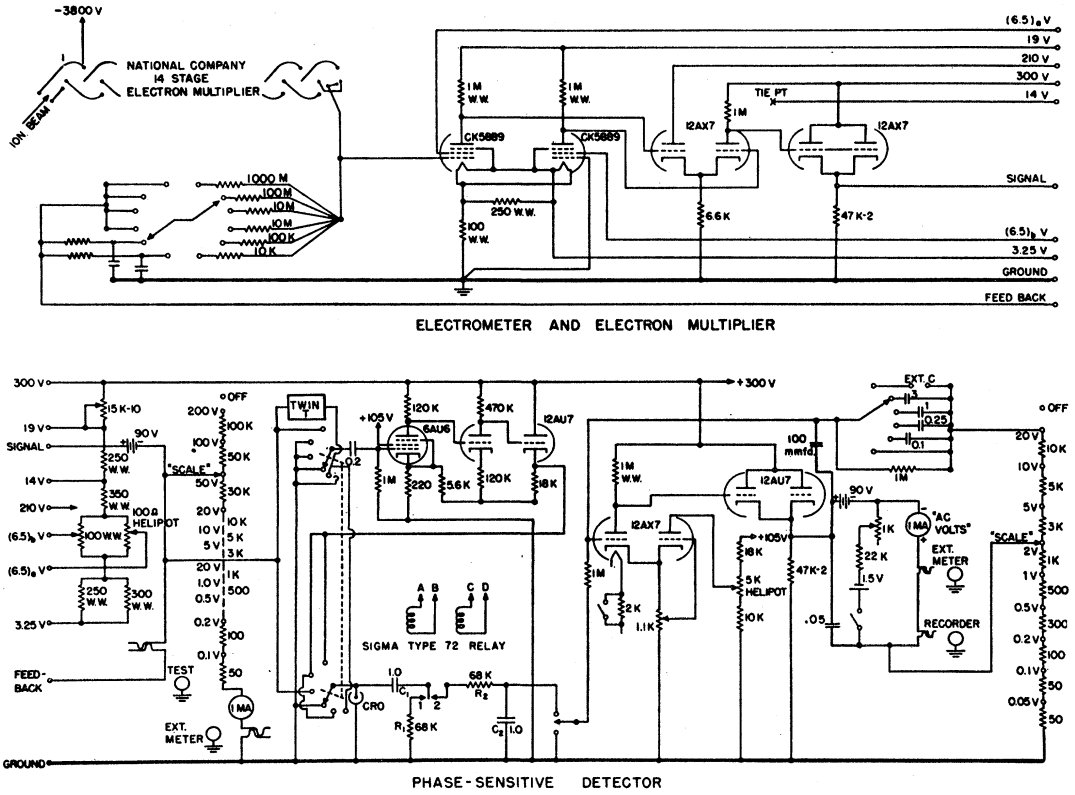

FIG. 3. Electrometer and phase-sensitive detector circuits.

other onto a plane removed from its magnetic field. Ions are deflected through 45° with a radius of curvature of 15 in. The Armco pole tips are mounted on the modified yoke of a large NMR electromagnet. Currents of up to six amperes produce up to 3600 gauss in the 1-in. spectrometer gap. The usual range of ion acceleration voltages is from 2000 to 5000 volts, and the entire mass spectrum from $M=1$ to 200 can be observed with a resolution of 1 in 50.

The ion beam in its focal plane is incident on the first dynode of an electron multiplier (National Company), which is operated at -3800 volts. This voltage gives the ions an additional acceleration, and increases secondary electron production efficiency. Amplification of the multiplier output current is accomplished by an electrometer circuit, using 100% feedback to linearize its response. The output dc voltage of the electrometer is displayed, and the ac modulated component amplified, rectified, and displayed by a phase-sensitive detector. The circuits are essentially identical to those designed by Collins and Quinn,[2] and are shown in Fig. 3. Provision is made for optional use of a variable-bandpass twin-T amplifier on the ac signal to prevent noise overloading of the lock-in detector. Demodulation of the signal is accomplished by a relay (Sigma 72) driven in synchronism with the modulation device, such as a beam chopper or rf switching relay.

Measurements of ion currents have indicated that the collection efficiency of the wide aperture mass spectrometer is $>50\%$, and that the over-all absolute ionization probability on a beam of HF is 10^{-3} to 10^{-4}.

III. THEORY

The HF molecule is characterized by the proton and fluorine spin angular moments, $\mathbf{I}_p$ and $\mathbf{I}_F$, and the rotational angular momentum $\mathbf{J}$ of the molecule as a whole. The Hamiltonian for such a system in an external magnetic field H can be written as:

$$\begin{aligned}\frac{\mathcal{H}}{h}=&-[1-\sigma_p(\mathbf{J})]a_p\frac{\mathbf{I}_p\cdot\mathbf{H}}{|\mathbf{H}|}-[1-\sigma_F(\mathbf{J})]a_F\frac{\mathbf{I}_F\cdot\mathbf{H}}{|\mathbf{H}|}\\&-[1-\sigma_J(\mathbf{J})]b\frac{\mathbf{J}\cdot\mathbf{H}}{|\mathbf{H}|}-c_p\mathbf{I}_p\cdot\mathbf{J}-c_F\mathbf{I}_F\cdot\mathbf{J}\\&+\frac{5d_1}{(2J-1)(2J+3)}[\tfrac{3}{2}(\mathbf{I}_p\cdot\mathbf{J})(\mathbf{I}_F\cdot\mathbf{J})\\&+\tfrac{3}{2}(\mathbf{I}_F\cdot\mathbf{J})(\mathbf{I}_p\cdot\mathbf{J})-(\mathbf{I}_p\cdot\mathbf{I}_F)\mathbf{J}^2]\\&-\frac{5f}{3(2J-1)(2J+3)}\left[3\frac{(\mathbf{J}\cdot\mathbf{H})^2}{|\mathbf{H}|^2}-\mathbf{J}^2\right]+\delta\mathbf{I}_p\cdot\mathbf{I}_F.\end{aligned}$$

The constants a_p and a_F represent the interaction of the proton and fluorine nuclear magnetic moments with

the external field[8]; b expresses the interaction of the rotational magnetic moment of the molecule with the external field; c_p and c_F, the spin-rotational constants, represent the interaction of the proton fluorine nuclear magnetic moments with the magnetic field at the position of the nuclei produced by the molecular rotation. d_1 consists mainly of the direct dipole-dipole interaction of the proton and fluorine magnetic moments; it also includes the tensor part of the electron-coupled spin-spin interaction, of which δ is the scalar part. f is the orientation-dependent part of the molecular diamagnetic interaction with the external field.

The Hamiltonian may also be written[5] in terms of the angular momentum operators, I^2, I_z, I_+, I_-, J^2, J_z, J_+, J_-. Using standard relations,[9] one may then obtain the diagonal and off-diagonal matrix elements of $\mathcal{H}$ in the high-field limit, where the three angular moments are essentially decoupled from each other. The matrix elements diagonal in m_p, m_F, m_J can be summarized as:

$$\frac{\langle\mathcal{H}\rangle}{h}=-[1-\sigma_p]a_p m_p-[1-\sigma_F]a_F m_F$$
$$-[1-\sigma_J]bm_J-c_p m_p m_J-c_F m_F m_J$$
$$+\frac{5d_1}{(2J-1)(2J+3)}m_p m_F[3m_J{}^2-J(J+1)]$$
$$-\frac{5f}{3(2J-1)(2J+3)}[3m_J{}^2-J(J+1)]+\delta m_p m_F.$$

Corrections to the high-field energy levels proportional, to $1/H$ may be calculated by substituting the off-diagonal matrix elements in the standard formula of second-order perturbation theory. The complete matrix may also be diagonalized to give the energy levels to higher accuracy. Taking the energy differences corresponding to $\Delta m_p=\pm1$, $\Delta m_F=0$, $\Delta m_J=0$ (proton "flops") and $\Delta m_F=\pm1$, $\Delta m_p=0$, $\Delta m_J=0$ (fluorine "flops") yields the frequencies of the expected transitions. The energy differences in second-order perturbation theory are given in Tables II and III for $J=0$, 1, 2. Table IV shows the expected intensities for transitions in a given J state, for two different source temperatures.

IV. EXPERIMENTAL PROCEDURE AND OBSERVATIONS

Hydrogen fluoride gas (commercial grade, anhydrous, Matheson Company) was introduced into the copper source through copper tubing and monel needle valves with Kel-F seals. Copper exposed to HF at atmospheric pressure becomes coated with a greenish layer of copper fluoride, which acts as a protective coat and inhibits further corrosion. It took considerable time initially to

[8] The notation and sign conventions here follow reference 5.
[9] J. M. B. Kellogg, I. I. Rabi, N. F. Ramsey, and J. R. Zacharias, Phys. Rev. **56**, 728 (1939); **57**, 677 (1940).

TABLE II. Proton transition frequencies for rotational states $J=0$, 1, and 2 through terms $\propto 1/H$, strong-field representation.

	m_J	m_F	
$J=0$	0	$+\frac{1}{2}$	$(1-\sigma_p)a_p-\frac{1}{2}\delta$
	0	$-\frac{1}{2}$	$(1-\sigma_p)a_p+\frac{1}{2}\delta$
$J=1$	$+1$	$+\frac{1}{2}$	$(1-\sigma_p')a_p+c_p-\frac{1}{2}d_1-\frac{1}{2}\delta+(+c_1+c_6)$
	$+1$	$-\frac{1}{2}$	$(1-\sigma_p')a_p+c_p+\frac{1}{2}d_1+\frac{1}{2}\delta+(-c_2+c_3+c_4+c_5+c_6)$
	0	$+\frac{1}{2}$	$(1-\sigma_p')a_p+d_1-\frac{1}{2}\delta+(+c_1+c_2+c_3-c_4+c_7)$
	0	$-\frac{1}{2}$	$(1-\sigma_p')a_p-d_1+\frac{1}{2}\delta+(+c_1+c_2+c_3-c_4+c_7)$
	-1	$+\frac{1}{2}$	$(1-\sigma_p')a_p-c_p-\frac{1}{2}d_1-\frac{1}{2}\delta+(-c_2+c_3+c_4+c_5+c_6)$
	-1	$-\frac{1}{2}$	$(1-\sigma_p')a_p-c_p+\frac{1}{2}d_1+\frac{1}{2}\delta+(+c_1+c_6)$
$J=2$	$+2$	$+\frac{1}{2}$	$(1-\sigma_p'')a_p+2c_p-(5/7)d_1-\frac{1}{2}\delta+(+k_1+k_4)$
	$+2$	$-\frac{1}{2}$	$(1-\sigma_p'')a_p+2c_p+(5/7)d_1+\frac{1}{2}\delta$ $+(+k_1-k_5+k_9+k_{10}+k_{11})$
	$+1$	$+\frac{1}{2}$	$(1-\sigma_p'')a_p+c_p+(5/14)d_1-\frac{1}{2}\delta$ $+(+k_2+k_4+k_5+k_6-k_{11})$
	$+1$	$-\frac{1}{2}$	$(1-\sigma_p'')a_p+c_p-(5/14)d_1+\frac{1}{2}\delta$ $+(+k_2+k_3-k_7+k_{10}+k_{12}+k_{13})$
	0	$+\frac{1}{2}$	$(1-\sigma_p'')a_p+(5/7)d_1-\frac{1}{2}\delta$ $+(+k_6+k_7+k_8+k_9+k_{12}-k_{13})$
	0	$-\frac{1}{2}$	$(1-\sigma_p'')a_p-(5/7)d_1+\frac{1}{2}\delta$ $+(+k_6+k_7+k_8+k_9+k_{12}-k_{13})$
	-1	$+\frac{1}{2}$	$(1-\sigma_p'')a_p-c_p+(5/14)d_1-\frac{1}{2}\delta$ $+(+k_2+k_3-k_7+k_{10}+k_{12}+k_{13})$
	-1	$-\frac{1}{2}$	$(1-\sigma_p'')a_p-c_p-(5/14)d_1+\frac{1}{2}\delta$ $+(+k_2+k_4+k_5+k_6-k_{11})$
	-2	$+\frac{1}{2}$	$(1-\sigma_p'')a_p-2c_p-(5/7)d_1-\frac{1}{2}\delta$ $+(+k_1-k_5+k_9+k_{10}+k_{11})$
	-2	$-\frac{1}{2}$	$(1-\sigma_p'')a_p-2c_p+(5/7)d_1+\frac{1}{2}\delta+(+k_1+k_4)$

$c_1=(-\frac{1}{2}\sqrt{2}c_p+\frac{3}{8}\sqrt{2}d_1)^2/(a_p-b)$
$c_2=(-\frac{1}{2}\sqrt{2}c_F+\frac{3}{8}\sqrt{2}d_1)^2/(a_F-b)$
$c_3=(-\frac{1}{2}\sqrt{2}c_p-\frac{3}{8}\sqrt{2}d_1)^2/(a_p-b)$
$c_4=(-\frac{1}{2}\sqrt{2}c_F-\frac{3}{8}\sqrt{2}d_1)^2/(a_F-b)$
$c_5=(\frac{3}{2}d_1)^2/(a_p+a_F-2b)$
$c_6=(-\frac{1}{4}d_1+\frac{1}{2}\delta)^2/(a_p-a_F)$
$c_7=(\frac{1}{2}d_1+\frac{1}{2}\delta)^2/(a_p-a_F)$

$k_1=[-(5/14)d_1+\frac{1}{2}\delta]^2(a_p-a_F)$
$k_2=[(5/28)d_1+\frac{1}{2}\delta]^2/(a_p-a_F)$
$k_3=[(15/14)d_1]^2/(a_p+a_F-2b)$
$k_4=[-c_p+(15/28)d_1]^2/(a_p-b)$
$k_5=[-c_F+(15/28)d_1]^2/(a_F-b)$
$k_6=[-\frac{1}{2}(\sqrt{6})c_p+(5/56)(\sqrt{6})d_1]^2/(a_p-b)$
$k_7=[-\frac{1}{2}(\sqrt{6})c_F+(5/56)(\sqrt{6})d_1]^2/(a_F-b)$
$k_8=[(5/14)d_1+\frac{1}{2}\delta]^2/(a_p-a_F)$
$k_9=\frac{2}{3}k_3=[(5/14)(\sqrt{6})d_1]^2/(a_p+a_F-2b)$
$k_{10}=[-c_p-(15/28)d_1]^2/(a_p-b)$
$k_{11}=[-c_F-(15/28)d_1]^2/(a_F-b)$
$k_{12}=[-\frac{1}{2}(\sqrt{6})c_p-(5/56)(\sqrt{6})d_1]^2/(a_p-b)$
$k_{13}=[-\frac{1}{2}(\sqrt{6})c_F-(5/56)(\sqrt{6})d_1]^2/(a_F-b)$

TABLE III. Fluorine transition frequencies for rotational states $J=0$, 1, and 2 through terms $\propto 1/H$, strong-field representation.

	m_J	m_p	
$J=0$	0	$+\frac{1}{2}$	$(1-\sigma_F)a_F-\frac{1}{2}\delta$
	0	$-\frac{1}{2}$	$(1-\sigma_F)a_F+\frac{1}{2}\delta$
$J=1$	+1	$+\frac{1}{2}$	$(1-\sigma_F')a_F+c_F-\frac{1}{2}d_1-\frac{1}{2}\delta+(+c_2-c_6)$
	+1	$-\frac{1}{2}$	$(1-\sigma_F')a_F+c_F+\frac{1}{2}d_1+\frac{1}{2}\delta+(-c_1+c_3+c_4+c_5-c_6)$
	0	$+\frac{1}{2}$	$(1-\sigma_F')a_F+d_1-\frac{1}{2}\delta+(c_1+c_2-c_3+c_4-c_7)$
	0	$-\frac{1}{2}$	$(1-\sigma_F')a_F-d_1+\frac{1}{2}\delta+(c_1+c_2-c_3+c_4-c_7)$
	−1	$+\frac{1}{2}$	$(1-\sigma_F')a_F-c_F-\frac{1}{2}d_1-\frac{1}{2}\delta+(-c_1+c_3+c_4+c_5-c_6)$
	−1	$-\frac{1}{2}$	$(1-\sigma_F')a_F-c_F+\frac{1}{2}d_1+\frac{1}{2}\delta+(+c_2-c_6)$
$J=2$	+2	$+\frac{1}{2}$	$(1-\sigma_F'')a_F+2c_F-(5/7)d_1-\frac{1}{2}\delta+(-k_1+k_5)$
	+2	$-\frac{1}{2}$	$(1-\sigma_F'')a_F+2c_F+(5/7)d_1+\frac{1}{2}\delta+(-k_1-k_4+k_9+k_{10}+k_{11})$
	+1	$+\frac{1}{2}$	$(1-\sigma_F'')a_F+c_F+(5/14)d_1-\frac{1}{2}\delta+(-k_2+k_4+k_5+k_7-k_{10})$
	+1	$-\frac{1}{2}$	$(1-\sigma_F'')a_F+c_F-(5/14)d_1+\frac{1}{2}\delta+(-k_2+k_3-k_6+k_{11}+k_{12}+k_{13})$
	0	$+\frac{1}{2}$	$(1-\sigma_F'')a_F+(5/7)d_1-\frac{1}{2}\delta+(+k_6+k_7-k_8+k_9-k_{12}+k_{13})$
	0	$-\frac{1}{2}$	$(1-\sigma_F'')a_F-(5/7)d_1+\frac{1}{2}\delta+(+k_6+k_7-k_8+k_9-k_{12}+k_{13})$
	−1	$+\frac{1}{2}$	$(1-\sigma_F'')a_F-c_F+(5/14)d_1-\frac{1}{2}\delta+(-k_2+k_3-k_6+k_{11}+k_{12}+k_{13})$
	−1	$-\frac{1}{2}$	$(1-\sigma_F'')a_F-c_F-(5/14)d_1+\frac{1}{2}\delta+(-k_2+k_4+k_5+k_7-k_{10})$
	−2	$+\frac{1}{2}$	$(1-\sigma_F'')a_F-2c_F-(5/7)d_1-\frac{1}{2}\delta+(-k_1-k_4+k_9+k_{10}+k_{11})$
	−2	$-\frac{1}{2}$	$(1-\sigma_F'')a_F-2c_F+(5/7)d_1+\frac{1}{2}\delta+(-k_1+k_5)$

fluoridize the surface. Thereafter the beam intensity increased greatly, so that the signal-to-noise ratio on the chopper-modulated beam was 30 to 1. Source pressure was monitored on an halogenated oil manometer, and its temperature regulated by adding cooled alcohol to the source trap.

In all of the work described in this paper, resonances were observed with only a single short ($\frac{3}{4}$ in.) rf coil. Because the expected linewidth using the single coil is about 24 kc/sec, the current regulator for the C field was not used. The small, slow drift of the voltage-regulated power supplies caused no difficulties, and the C field was calibrated by the proton and fluorine moments to a higher precision than was required. Off-on rf modulation (using Western Electric 276E relays) provided lock-in detection. The mass spectrometer was tuned to mass 20, corresponding to HF^+ion.

The first data taken was with a C field of about 900 gauss. Eight distinct peaks were observed about the $J=0$ fluorine and proton resonances. The proton and fluorine magnetic moments are quite close in value, which indicated that the $\Delta m_p=\pm 1$, and $\Delta m_F=\pm 1$ transitions were badly overlapped, complicating interpretation. To overcome this, observations were then made at 1800 and 3600 gauss to separate the spectra. The best data taken were at 3600 gauss, where the corrections proportional to $1/H$ are small, and the signal-to-noise ratio appeared best. Figures 4(A) and 5(A) show typical recorder tracings of the proton and fluorine spectra, with a lock-in time constant of eight seconds. The maximum resonance amplitude corresponds to 6% of the total beam intensity. The proton spectrum is seen to consist of five distinct major peaks and some lesser side structure. The fluorine spectrum consists of sets of doublet side peaks spaced about 300 kc/sec either side of the central fluorine resonance.

V. INTERPRETATION AND RESULTS

The values of the constants $|c_p|$, $|c_F|$, and d_1 were determined from the positions and shapes of the resonances. Effects resulting from the signs of these constants enter only into the small terms proportional to $1/H$, and can be largely eliminated by differencing selected pairs of transition frequencies.

The line separation of approximately 300 kc/sec above and below the central fluorine frequency can be ascribed to the spin-rotational constant c_F. Further evidence is afforded by a doublet appearing about 600 kc/sec above, which is consistent with the hypothesis that it corresponds to $|m_J|=2$, about $2c_F$ above the central frequency. The splitting of the fluorine resonances into doublets is due to d_1, and arises from $m_p=\pm\frac{1}{2}$. Averaging and differencing frequencies gives the results $|c_F|=305\pm 2$ kc/sec, and $d_1-\delta/2=57\pm 2$ kc/sec. The latter is in excellent agreement with a calculated estimate.

The appearance of four major side peaks about the central $J=0$ proton peak can only be consistently explained by a value of $|c_p|\approx 70$ kc/sec, in combination with $d_1=57$ kc/sec. In this case each of the two side

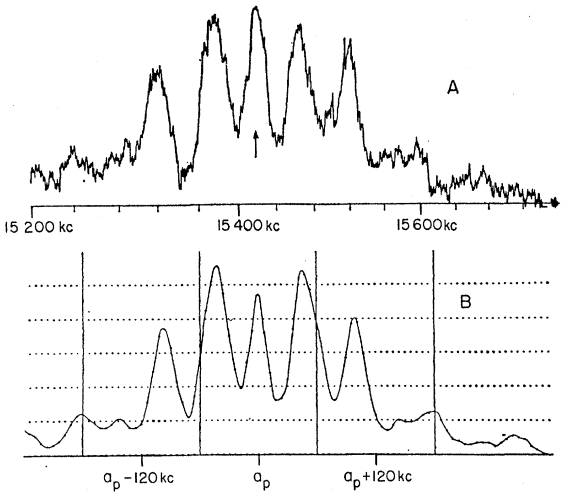

FIG. 4. Proton transition resonance spectrum, source temperature $=-55$°C. (A) Experimental results, lock-in time constant $=8$ sec. (B) Theoretical results, using Univac solution of the secular equation, through $J=5$.

peaks adjacent to the central peak are composed of two $J=1$ transitions and the outer two peaks have only one $J=1$ transition apiece. The frequency difference between the outer two peaks of 200 kc/sec $\approx 2|c_p|+d_1+\delta$ implies $|c_p|=71\pm 3$ kc/sec.

The above analysis includes effects of only the $J=0$ and $J=1$ states; it further neglects effects of second and higher order perturbations. A numerical analysis shows that the dominant features of the experimental curves can be interpreted in this fashion. However, the best support for the correctness of our choice of parameters is a set of calculated curves using the constants given above to predict the observed line shapes. One of the authors (N.F.R.) has written several Univac programs, which calculate the frequencies and weights of spin transitions, both exactly through solution of the secular equation, and approximately, using perturbation theory. He has also devised a program which folds together the weighted transitions for a given experimental resonance width, and prints out a point plot of the resonance shapes. Since these calculations include the effect of all significant J states, their results confirm the correctness of the above simplified interpretation. Presentation of all the results of calculations on HF are beyond the scope of the present paper, but one can summarize the conclusions as follows:

1. The determination of the signs of c_p and c_F has not been possible at high fields and low resolution, as there was insufficient difference between the curves calculated for the four possible combinations of signs of c_p and c_F.

2. The calculated fluorine spectrum at high fields is in good agreement with that observed. In particular, the experimentally observed phenomenon of the higher frequency part of an m_J doublet being higher in intensity is clearly shown.

3. The calculated proton spectrum is in good agreement with the observed spectrum. The five proton peaks only occur with the proper spacing and relative intensities for $|c_p|\approx 70$ kc/sec.

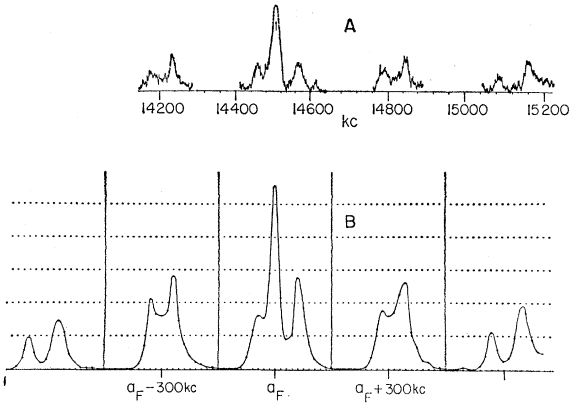

FIG. 5. Fluorine transition resonance spectrum, source temperature $=-55$°C. (A) Experimental results, lock-in time constant $=8$ sec. (B) Theoretical results, using Univac solution of the secular equation, through $J=5$.

TABLE IV. Individual proton and fluorine transition intensities, relative to total beam. (Throw-out power $=0.5$.)

J	$T=195$°K	$T=284$°K
0	2.81%	1.44%
1	2.06%	1.23%
2	1.10%	0.90%
3	0.43%	0.57%
4	0.12%	0.30%
5	0.03%	0.13%

4. The assumption that the spacing between the outer two proton peaks is $2|c_p|+d_1+\delta$ was verified by calculating the proton spectrum for differing values of $|c_p|$ and observing how the spacing alters with $|c_p|$.[10]

5. The effect of assuming varying value for the rotational magnetic moment was negligible.

Calculated proton and fluorine resonance curves using our best values of the molecular interaction constants are shown in Figs. 4(B) and 5(B), and may be compared with the experimental results. Agreement is gratifyingly close.

VI. DISCUSSION

The spin-rotational interaction constants correspond to magnitudes of the rotational magnetic fields at the nuclei of 16.7 gauss at the proton and 76.1 gauss at the fluorine per unit rotational quantum number. The fluorine spin-rotational constant is the largest yet observed. Its exceptional magnitude may be ascribed to the combination of (a) the low molecular moment of inertia and (b) the electron distribution about the fluorine, which reacts strongly to the rotational perturbation. The latter property appears in other fluorides. For example, using $c_F=-32.9$ kc/sec in Li^7F,[11] one finds that if Li^7F rotated at the same angular velocity as HF, its rotational magnetic field at the F would be even larger (119 gauss).

The origin of the rotational field is twofold.[12] First, the rotation of one charged nucleus about the other is equivalent to a field-producing current. Secondly, rotation of the molecule can be considered to perturb the $^1\Sigma$ ground electronic state of the molecule and to mix in a small amount of higher lying magnetic $^1\Pi$ states. A calculation of the nuclear contribution is simple. In combination with our data, it shows that in HF, the electronic contribution outweighs the nuclear six to one. An *ab initio* calculation of the electronic contribution involves the evaluation of high-frequency terms[5] involving the excited Π states. The results are unreliable and extremely sensitive to the Π functions chosen. Models based on a simpler approach, such as the irrotational-flow model of Espe[12] and Wick[13] give good

[10] The value of $\delta=0.615$ kc/sec assumed has been that measured by I. Solomon and N. Bloembergen, J. Chem. Phys. **25**, 261 (1956).
[11] R. Braunstein and J. Trischka, Phys. Rev. **98**, 1092 (1955).
[12] I. Espe, Phys. Rev. **103**, 1254 (1956).
[13] G. C. Wick, Phys. Rev. **73**, 51 (1948).

(10%) agreement in hydrogen, but somewhat less satisfactory results for a larger, many-electron model like HF.[14]

The data so far obtained at high fields has not allowed a determination of the signs of c_F and c_p. In principle, the asymmetries produced by second-order perturbations should make the sign determination possible; but the effects are small and only slightly affect the intensities of the present resonances, rather than the positions of the maxima. The sign of c_F should be the same as that of the high-frequency electronic terms since the magnitude of c_F is so much greater than the nuclear contribution. All available experimental data on spin-rotational constants shows that the sign of the electronic contribution is that corresponding to the electrons following the molecular rotation. In this case, using our convention,[5] the sign of c_F would be negative. It should be pointed out, however, that, in principle, the sign of the high-frequency term in the expression for the spin-rotational interaction cannot be determined except through explicit evaluation. This is fundamentally different from the case of the high-frequency electronic terms which contribute to the rotational magnetic moment and diamagnetic susceptibility, and are positive-definite in form. Further experiments with higher resolution are planned, and it is hoped that these will provide the signs of c_p and c_F.

In past applications of theories of relaxation times in nuclear magnetic resonance experiments, the spin-rotational interaction has ordinarily been neglected. Therefore, with the value of the fluorine spin-rotational interaction constant being much greater than the nuclear-spin interaction in the same molecule, it might be expected that the relaxation time would dominantly be determined by the spin-rotational interaction. However, on the basis of calculations and discussion with Purcell and Bloembergen, it appears that if the spin-rotational interaction is included, the agreement between theoretical and experimental relaxation times[10] in liquid HF is made worse rather than improved. This is in contrast to a measurement we have recently made but not yet reported on the spin-rotational interaction in SF_6. In this latter case, the inclusion of the spin-rotational interaction brings about a much better agreement between the experimental relaxation time[15] and the theoretical value. The probable difference between the two cases is that with liquid HF the molecule is sufficiently asymmetric and sufficiently closely surrounded by nearby neighbors that the molecular rotation is dominantly quenched,[16] so the spin-rotational interaction does not contribute significantly to the relaxation time. On the other hand, with gaseous SF_6 the combination of the greater spherical symmetry and the greater intermolecular spacing allows a single rotation state to be preserved sufficiently long that the rotational magnetic field can contribute importantly to the relaxation process. There are no published data on nuclear relaxation in gaseous HF so it is not yet possible to determine experimentally whether merely passing to the gaseous state with this molecule will diminish the quenching sufficiently for the spin-rotational interaction to contribute importantly to the nuclear relaxation.

ACKNOWLEDGMENTS

The authors wish to thank K. T. Bainbridge, E. M. Purcell, and N. Bloembergen for their advice and assistance.

[14] Baker, reference 6.

[15] J. Schwartz and E. M. Purcell (private communication).

[16] J. H. Van Vleck, *The Theory of Electric and Magnetic Susceptibilities* (Oxford University Press, New York, 1932), pp. 287 ff.